nature materials

LETTERS

PUBLISHED ONLINE: 7 DECEMBER 2015 | DOI: 10.1038/NMAT4487

Molecular design and control of fullerene-based bi-thermoelectric materials

Laura Rincón-García[1,2], Ali K. Ismael[3,4], Charalambos Evangeli[1], Iain Grace[3], Gabino Rubio-Bollinger[1,5], Kyriakos Porfyrakis[6], Nicolás Agraït[1,2,5*] and Colin J. Lambert[3*]

Molecular junctions are a versatile test bed for investigating nanoscale thermoelectricity[1–10] and contribute to the design of new cost-effective environmentally friendly organic thermoelectric materials[11]. It was suggested that transport resonances associated with discrete molecular levels could play a key role in thermoelectric performance[12,13], but no direct experimental evidence has been reported. Here we study single-molecule junctions of the endohedral fullerene $Sc_3N@C_{80}$ connected to gold electrodes using a scanning tunnelling microscope. We find that the magnitude and sign of the thermopower depend strongly on the orientation of the molecule and on applied pressure. Our calculations show that Sc_3N inside the fullerene cage creates a sharp resonance near the Fermi level, whose energetic location, and hence the thermopower, can be tuned by applying pressure. These results reveal that $Sc_3N@C_{80}$ is a bi-thermoelectric material, exhibiting both positive and negative thermopower, and provide an unambiguous demonstration of the importance of transport resonances in molecular junctions.

The design of new thermoelectric materials for converting waste heat directly into electricity is a global challenge[14]. A successful strategy for improving thermoelectric properties of inorganic semiconductors is nanostructuring, which leads to quantum confinement of electrons and suppression of parasitic phonons[15]. However, the cost and toxicity of available inorganic thermoelectric devices at present are problematic and make organic thermoelectrics particularly attractive for sustainable waste energy conversion[11]. Recently, the ability to measure the thermoelectric properties of single molecules has begun to deliver the fundamental physical and chemical knowledge that will be needed to design new materials and build devices suitable for applications. It has been demonstrated both experimentally and theoretically that, at a molecular scale, the thermopower S can be controlled by varying the chemical composition[1], varying the position of intramolecular energy levels relative to the work function of metallic electrodes[2,3], systematically increasing the single-molecule lengths and varying the binding groups within a family of molecules[4–8], by tuning the interaction between two neighbouring molecules[9], and by controlling the transport properties with an electrostatic gate[10] or electrochemically[16]. These single-molecule experiments yielded room-temperature values of S ranging in magnitude from about 1 to 50 $\mu V\,K^{-1}$.

A key factor in determining the thermoelectric performance of a molecular junction, according to theoretical calculations, is the presence of transport resonances close to the Fermi level. The effect of transmission resonances was explored theoretically by Finch *et al.*[12]. In this work the resonances were introduced by quantum interference effects due to the addition of side groups to the molecular backbone. The resulting Fano resonance near the Fermi level leads to a large enhancement in the thermopower and thermoelectric efficiency. Enhanced thermoelectric properties have also been predicted in the vicinity of interference-induced transmission nodes[13]. However, this approach remains experimentally unexplored.

Our recent experiments and theory of C_{60}-based thermoelectricity[9] and other studies[2,3,10] showed that C_{60} is a robust thermoelectric material, with a consistently negative thermopower, which originates from the presence of a broadened lowest unoccupied molecular orbital (LUMO) level near the Fermi energy E_F whose monotonic shape makes it difficult to vary the sign of S. Therefore we reasoned that if a narrower transport resonance could be created within the tail of the LUMO, this could lead to increased tunability. To create such a feature, we selected the endohedral fullerene $Sc_3N@C_{80}$, which is known to have a relatively small energy gap[17] and is particularly stable at room temperature and above[18]. As shown below, the presence of the Sc_3N inside the fullerene cage not only creates the desired resonance, but also, depending on the orientation of the molecule, allows tuning of the resonance energy and hence the sign of the thermopower by mechanically compressing the junction. This experimental tuning of the sign of S by mechanical gating is unprecedented and is the first example of a bi-thermoelectric material, which can exhibit thermopower of either sign, without doping and without a change of chemical composition. Mechanical modulation of the thermopower of molecular junctions has been theoretically predicted[19]; however, as we will show, the origin of this effect is different.

In this Letter, we use a modified scanning tunnelling microscope (STM; ref. 9) to study single-molecule junctions of an endohedral fullerene $Sc_3N@C_{80}$ between gold electrodes. $Sc_3N@C_{80}$ consists of a fullerene cage (C_{80}-Ih) encapsulating three scandium atoms joined to one nitrogen, as shown schematically in Fig. 1a. Supplementary Fig. 1 and Methods contain more information about molecule purification and deposition. All STM experiments were performed at room temperature and in ambient conditions. STM imaging after deposition shows isolated molecules as well as aggregates at step edges or in small islands (Fig. 1b–d). Tunnelling spectroscopy on different isolated molecules reveals an asymmetric current–voltage characteristic (rectifying behaviour). We found that some

[1]Departamento de Física de la Materia Condensada and Condensed Matter Physics Center (IFIMAC), Universidad Autónoma de Madrid, E-28049 Madrid, Spain. [2]Instituto Madrileño de Estudios Avanzados en Nanociencia IMDEA-Nanociencia, E-28049 Madrid, Spain. [3]Department of Physics, Lancaster University, Lancaster LA1 4YW, UK. [4]Department of Physics, College of Education for Pure Science, Tikrit University, Tikreet 34001, Iraq. [5]Instituto Universitario de Ciencia de Materiales Nicolás Cabrera, Universidad Autónoma de Madrid, E-28049 Madrid, Spain. [6]Department of Materials, University of Oxford, Oxford OX1 3PH, UK. *e-mail: nicolas.agrait@uam.es; c.lambert@lancaster.ac.uk

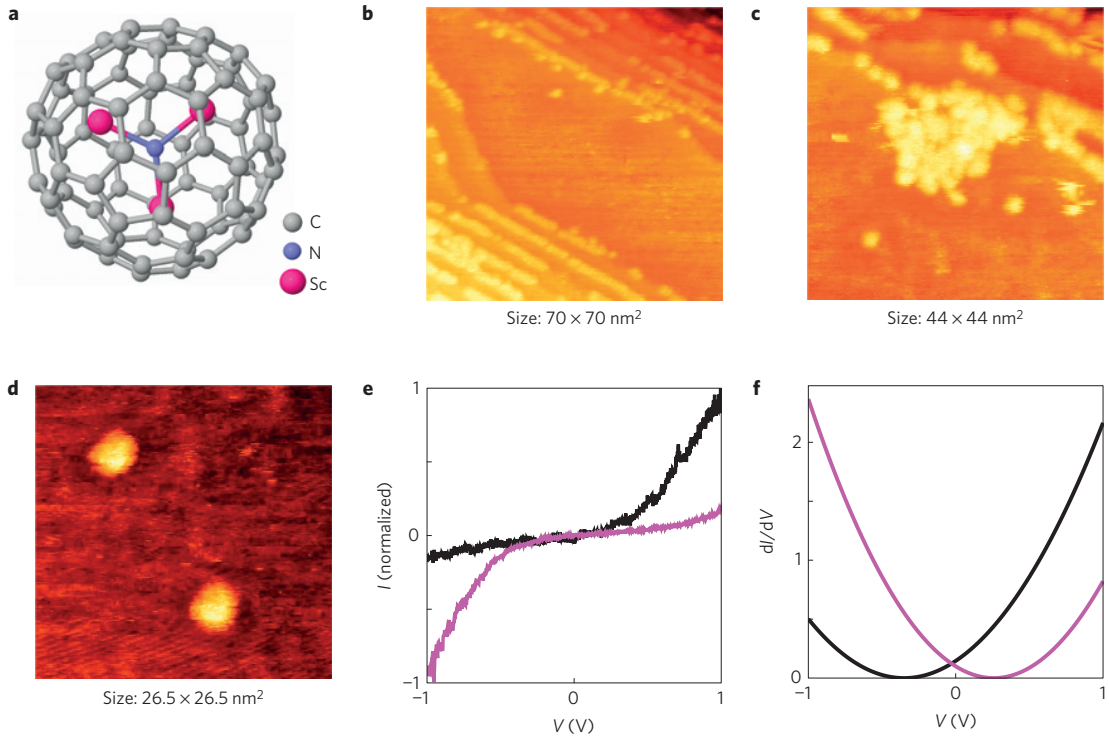

Figure 1 | Scanning tunnelling microscope images and tunnelling spectroscopy. a, Schematic of the endohedral fullerene $Sc_3N@C_{80}$ used in this work; notice the Sc_3N in the centre of the fullerene cage. **b**–**d**, STM images of the molecules on atomically flat (111) Au surfaces showing preferential adsorption at step edges (**b**), islands (**c**) and isolated molecules (**d**). **e**,**f**, *I*–*V* characteristics (**e**) and differential conductance (**f**) in the tunnelling regime on two different molecules of $Sc_3N@C_{80}$, presenting opposite rectifying behaviour.

molecules have higher conductance for positive voltage (black curve in Fig. 1e,f), similar to what is observed in C_{60}, whereas others have higher conductance for negative voltage (pink curve in Fig. 1e,f). This variation in the electronic behaviour of particular molecules of $Sc_3N@C_{80}$ has been reported in ultrahigh vacuum experiments[18] and has been attributed to the orientation of the molecule on the surface.

Next we measured simultaneously the conductance G and thermopower S of isolated $Sc_3N@C_{80}$ molecules (usually sitting on a step edge) as described in ref. 9 (Fig. 2c; see also Methods and Supplementary Figs 2 and 3). Fig. 2a,b show examples of G (in blue) and S (in green) curves measured on two different junctions while the tip approaches to touch the molecule. We found that the conductance of $Sc_3N@C_{80}$ behaves similarly to the case of C_{60} junctions, with a jump-to-contact signalling the first contact as the tip atoms touch the molecule. Typical values for the first-contact conductance are smaller by a factor of three than for C_{60} (as shown in Fig. 2d). The thermopower at first contact of $Sc_3N@C_{80}$ molecules, in contrast to C_{60}, can be positive, negative, or close to zero, depending on the selected molecule (Fig. 2a,b), resulting in a broad histogram centred around zero, as shown in Fig. 2e.

Interestingly, we find a correlation with the tunnelling spectroscopy results: molecules for which the conductance is higher at positive voltage show negative thermopower at first contact, whereas molecules for which the conductance is higher at negative voltage show positive thermopower. This is consistent with the fact that the thermoelectric properties of a molecular junction depend on the magnitude and derivative of the transmission at the Fermi level of the electrodes[20],

$$S = -\frac{\pi^2 k_B^2 T}{3e} \frac{\mathrm{d}\ln \mathcal{J}(E)}{\mathrm{d}E}\bigg|_{E=E_F} \quad (1)$$

where $\mathcal{J}(E)$ is the junction transmission, which is dependent on electron energy E, k_B is the Boltzmann constant, T is the average temperature of the junction, and e is the charge of the electron.

We now investigate the variation of thermopower as the tip advances after the first contact, compressing the $Sc_3N@C_{80}$ molecule. We positioned the tip on a selected isolated molecule and performed small amplitude (<0.5 nm) compression (approach–retraction) cycles, always maintaining contact with the molecule (see Supplementary Fig. 4). In these cycles a variable pressure is exerted on the molecule by the STM tip. In Fig. 3a,b, we present the simultaneous variations of G and S measured during three cycles for three different molecules. The periodic nature of these curves indicates that, in response to the pressure, the junction, that is, the molecule and the gold electrodes, deforms elastically. Larger amplitude (>0.5 nm) cycles destroy this periodicity, indicating the onset of plastic deformation (atomic rearrangements) in the gold electrodes[21] (see Supplementary Fig. 5 for further details). Taking into account previous results for gold contacts[22] and the fact that fullerene molecules are much stiffer than gold[23], we can safely assume that most of the elastic deformation corresponds to the electrodes and that the maximum pressure at the junction during our measurements is about 4 GPa (ref. 21).

The traces shown in Fig. 3a–c correspond to three molecules with different behaviours: the red traces correspond to a molecule which showed large positive thermopower at first contact (molecule 1); the blue traces, to a molecule with small positive thermopower (molecule 2); and the green traces, to a molecule with almost zero thermopower (molecule 3). We observe that, for all molecules, both the conductance and thermopower vary monotonically with pressure: the conductance increases and the thermopower decreases, becoming more negative, as the tip presses the molecule. This behaviour of the conductance is to be expected, because pressing will result in an increased coupling and, consequently, a larger conductance. However, the behaviour of the thermopower is most unusual: very large variations are observed and even a change

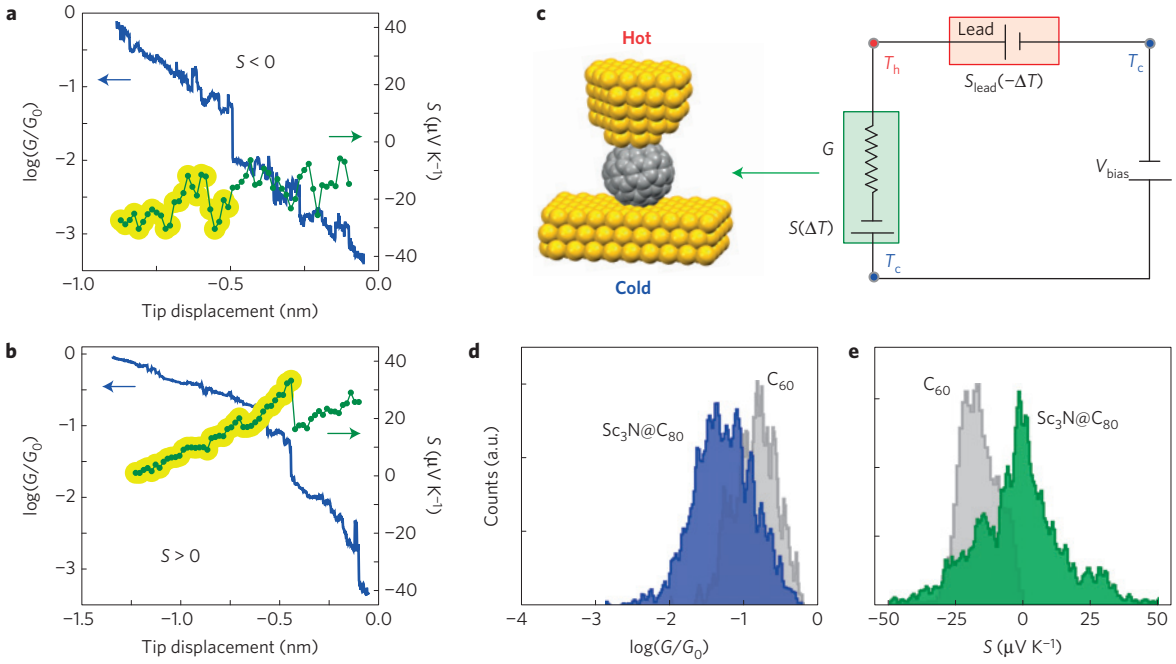

Figure 2 | Thermopower and conductance simultaneous measurements. a,**b**, Conductance, G (blue), and thermopower, S (green), simultaneously acquired while approaching individual $Sc_3N@C_{80}$ molecules. For the molecule in **a** the thermopower is always negative, whereas for the molecule in **b** it is always positive. In these measurements the temperature difference was $\Delta T \simeq 40$ K. The conductance quantum is $G_0 = 2e^2/h$, where e is the electron charge and h is Planck's constant. The portion of the thermopower trace highlighted in yellow corresponds to molecular contact with the tip. **c**, Schematic representation of the experimental set-up. The tip is heated to a temperature T_h above ambient temperature T_c, while the substrate is maintained at T_c (see Supplementary Fig. 3 for more details of the thermal circuit). **d**,**e**, Histograms of conductance G (**d**, blue) and thermopower S (**e**, green) at first contact for $Sc_3N@C_{80}$ compared to the values for C_{60} (in grey). For the $Sc_3N@C_{80}$ histograms, the mean conductance value is $\bar{G} = 0.05G_0$ and the mean thermopower is $\bar{S} = -2\,\mu V\,K^{-1}$.

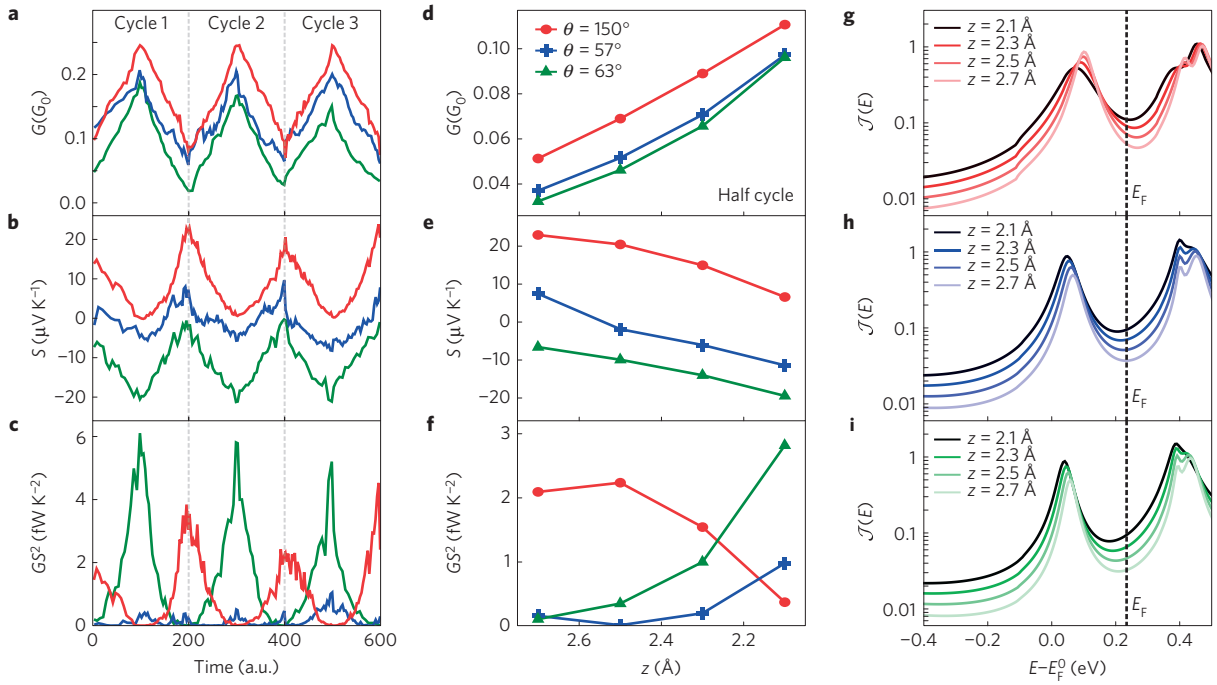

Figure 3 | Effect of pressure on $Sc_3N@C_{80}$ molecular junctions. a–c, Periodical variations of the conductance G, thermopower S and power factor GS^2, as the STM tip advances and retracts during three cycles. Each half cycle corresponds to less than 0.5 nm. Each colour corresponds to a different molecule. **d–f**, Calculated G, S and GS^2, for three different orientations (θ) as the tip–molecule separation z decreases from 2.7 Å to 2.1 Å, which corresponds to increasing pressure in the first half of experimental cycles. The orientations have been chosen such as to present similar amplitude variations to the experimental curves. **g–i**, Transmission curves, $\mathcal{T}(E)$, for the same three different orientations ($\theta = 150°$, $\theta = 57°$, and $\theta = 63°$, respectively) and for different z values. The Fermi level is shifted from the position given by density functional theory (DFT) and the black dotted line indicates the true Fermi level, as explained in the text (see also Supplementary Figs 9 and 10).

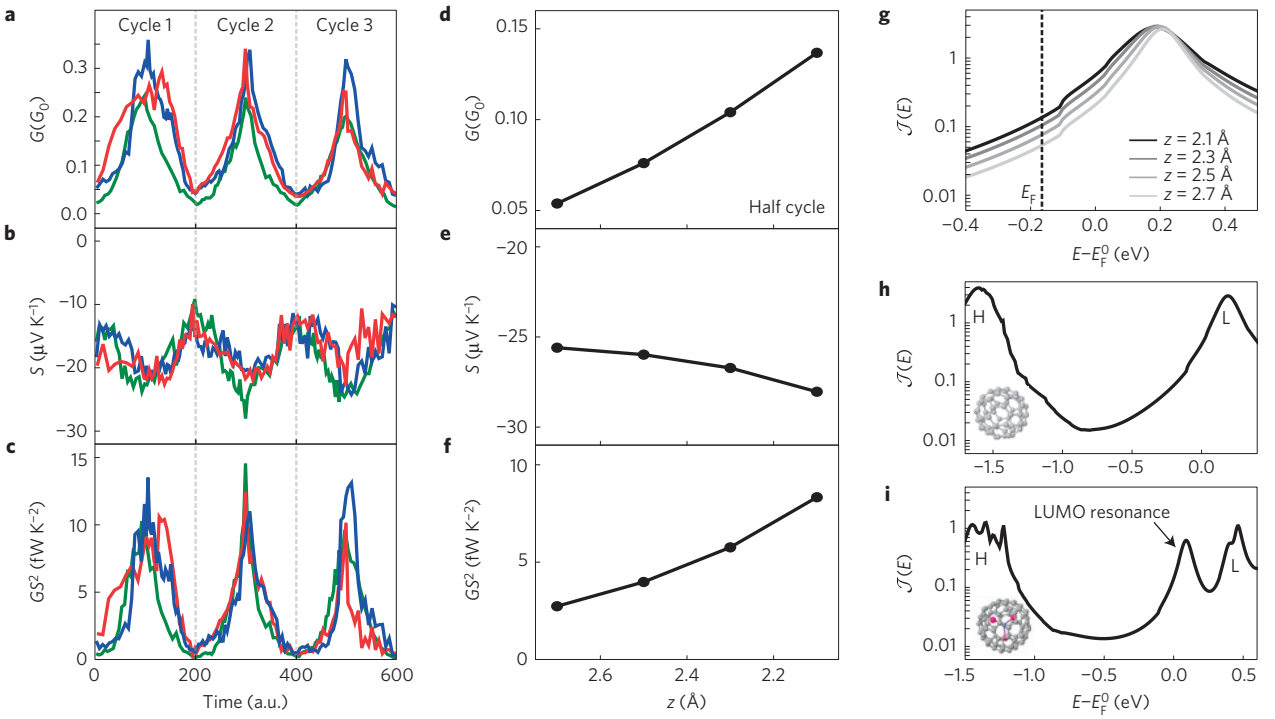

Figure 4 | Effect of pressure on C_{60} molecular junctions and comparison with $Sc_3N@C_{80}$ junctions. a–c, Periodical variations of the conductance, *G*, thermopower, *S*, and power factor, GS^2, of C_{60}, as the STM tip advances and retracts during three cycles. Each colour corresponds to a different molecule. Each half cycle corresponds to less than 0.5 nm. **d–f**, Calculated *G*, *S* and GS^2, as the tip–molecule separation, *z*, decreases from 2.7 Å to 2.1 Å, which corresponds to increasing pressure in the first half of experimental cycles. **g**, Transmission curves, $\mathcal{T}(E)$, for different *z* values. The Fermi level is shifted from the position given by DFT and the black dotted line indicates the true Fermi level, as explained in the text. In this case, $E_F = E_F^0 - 0.165$ eV, chosen such as to present similar amplitude variations to the experimental curves. **h**,**i**, Transmission curves, $\mathcal{T}(E)$, for C_{60} and $Sc_3N@C_{80}$ junctions, respectively. Letters H and L indicate the highest occupied molecular orbital (HOMO) and LUMO peaks of the fullerene cages. The main difference between both systems is the resonance present in the case of the endohedral fullerene.

in sign for molecule 2. This extreme sensitivity of thermopower of molecular junctions to pressure has never been reported and has a marked effect on the power factor, GS^2, as shown in Fig. 3c. For molecule 1, the power factor decreases with compression, whereas for molecule 2, it increases, reaching values of around 5 fW K^{-2}. In contrast, for molecule 3, GS^2 remains small during the whole cycle.

To elucidate the origin of the bi-thermoelectric effect of the endohedral fullerene junctions we use density functional theory (DFT) to simulate the contact and pressing of the $Sc_3N@C_{80}$ molecule. Using a combination of the quantum transport code Gollum[24] and the DFT code SIESTA (ref. 25), we calculate both the conductance and thermoelectric properties of the molecule contacted between gold electrodes (a detailed description can be found in the Supplementary Information). Three major inputs enter into the simulations. The first is the position of the molecule with respect to the electrodes *z*. We explore the effect of pressure on the transport properties by varying *z* around the equilibrium distance, which is found to be approximately 2.3 Å (see Supplementary Fig. 6). The orientation of the whole molecule is kept fixed while *z* is varied. A second input to the simulations is the orientation of the molecule with respect to the gold surface. The electronic structure of the isolated molecule shows a LUMO resonance located primarily on the Sc_3N molecule (see Supplementary Fig. 7); therefore, transport properties are expected to depend on the orientation of the Sc_3N, locked in position within the fullerene cage (see Supplementary Fig. 8), with respect to the gold surface. We define $\theta = 0°$ to be the orientation when the plane of the Sc_3N molecule is normal to the gold surface, such that at $\theta = 90°$ the Sc_3N is parallel to the surface (see Supplementary Fig. 6). To explore a range of orientations, we rotate through 180°, at intervals of 3°, and at each angle compute the zero-bias transmission coefficient $\mathcal{T}(E)$ (Supplementary Fig. 9). A third important input to the simulations is the energetic location of the molecular energy levels relative to the Fermi energy of the electrodes, because the conductance and thermopower are related to the value of the transmission and its derivative at the Fermi energy. As the DFT-predicted value E_F^0 is not reliable, to find the true Fermi level, we compute the transmission as a function of the energy for different orientations and pressures (see Fig. 3g–i and Supplementary Figs 9 and 10) and identify a single Fermi energy that reproduces the experimentally observed behaviour—that is, the thermopower is either positive or negative and always decreases, shifting to more negative values, as the molecule is pressed, in some cases passing through zero. We find that the true Fermi level is located between the LUMO resonance and the LUMO and takes a value $E_F = E_F^0 + 0.23$ eV.

With this choice of E_F, Fig. 3d–f shows *G*, *S* and GS^2, as a function of *z*, for three different orientations of the endohedral molecule ($\theta = 150°$ in red, $\theta = 57°$ in blue, and $\theta = 63°$ in green), which match the experimental behaviour of molecules 1, 2 and 3 in Fig. 3a–c. These results illustrate that the diverse experimental behaviours can be attributed to different orientations of the endohedral fullerene and reflect the shift towards negative values of the thermopower with pressure. The origin of this effect lies in the extreme sensitivity to pressure and orientation of the transmission function $\mathcal{T}(E)$, due to the presence of the resonance close to the Fermi level (Fig. 3g–i). For all the orientations (Supplementary Fig. 11), as the tip advances, the resonance becomes broadened and shifts to lower energies, as a consequence of changes in the imaginary and real parts, respectively, of the self-energy[26]—that is, in the coupling of the molecule to the electrodes. This results in an increase of the value

of the conductance, whereas the value of the thermopower becomes more negative as the molecule is pressed. For certain orientations, the junction shows a small positive thermopower and pressing the molecule produces an S that varies from positive to negative values (Fig. 3h), in good agreement with experimental results.

To further illustrate the formation of the LUMO resonance due to the Sc_3N, we have performed the same experiments on C_{60} junctions (Fig. 4a–c). We find that the thermopower is negative during the whole cycle and the power factor increases with compression to values $\sim$10 fW K^{-2}. Theoretical calculations show that for C_{60} junctions the Fermi level is always located in the smooth, increasing slope of the LUMO peak (see Fig. 4d–g). Figure 4h,i shows the transmission functions of C_{60} and $Sc_3N@C_{80}$ junctions, respectively, clearly showing that the main difference between these two systems is the LUMO resonance in the case of the endohedral fullerene.

Our calculations reveal the essential role played by the coupling of the molecule to the electrodes in the observed changes in the thermopower, whereas the deformation of the molecule plays only a minor role, in contrast to the mechanism proposed in ref. 19, which relied in intramolecular deformation.

In conclusion, we have demonstrated a new concept of bi-thermoelectricity, in which the sign and magnitude of the thermopower of a given material can be tuned. This effect was realized by identifying a molecule with a transmission resonance close to the Fermi energy, whose energetic location is sensitive to orientation and pressure. In this paper, we demonstrated bi-thermoelectricity in $Sc_3N@C_{80}$, but more generally the effect should be present in any material with orientation-dependent and pressure-dependent transmission resonances which can be caused to pass through the Fermi energy. For the future, if appropriate templating strategies could be implemented to select appropriate orientations of such molecules, then single-material, nanoscale tandem devices with alternating-sign thermopowers could be realized.

Methods

Methods and any associated references are available in the online version of the paper.

Received 16 July 2015; accepted 26 October 2015; published online 7 December 2015

References

1. Baheti, K. *et al*. Probing the chemistry of molecular heterojunctions using thermoelectricity. *Nano Lett.* **8**, 715–719 (2008).
2. Yee, S. K., Malen, J. A., Majumdar, A. & Segalman, R. Thermoelectricity in fullerene metal heterojunctions. *Nano Lett.* **11**, 4089–4094 (2011).
3. Lee, S. K., Ohto, T., Yamada, R. & Tada, H. Thermopower of benzenedithiol and C_{60} molecular junctions with Ni and Au electrodes. *Nano Lett.* **14**, 5276–5280 (2014).
4. Malen, J. A. *et al*. Identifying the length dependence of orbital alignment and contact coupling in molecular heterojunctions. *Nano Lett.* **9**, 1164–1169 (2009).
5. Tan, A. *et al*. Effect of length and contact chemistry on the electronic structure and thermoelectric properties of molecular junctions. *J. Am. Chem. Soc.* **133**, 8838–8841 (2011).
6. Balachandran, J., Reddy, P., Dunietz, B. D. & Gavini, V. End-group-induced charge transfer in molecular junctions: Effect on electronic-structure and thermopower. *J. Phys. Chem. Lett.* **3**, 1962–1967 (2012).
7. Widawsky, J. R. *et al*. Length-dependent thermopower of highly conducting Au–C bonded single molecule junctions. *Nano Lett.* **13**, 2889–2894 (2013).
8. Chang, W. B. *et al*. Controlling the thermoelectric properties of thiophene-derived single-molecule junctions. *Chem. Mater.* **26**, 7229–7235 (2014).
9. Evangeli, C. *et al*. Engineering the thermopower of C_{60} molecular junctions. *Nano Lett.* **13**, 2141–2145 (2013).
10. Kim, S., Jeong, W., Kim, K., Lee, W. & Reddy, P. Electrostatic control of thermoelectricity in molecular junctions. *Nature Nanotech.* **9**, 881–885 (2014).
11. Zhang, Q., Sun, Y., Xu, W. & Zhu, D. Organic thermoelectric materials: Emerging green energy materials converting heat to electricity directly and efficiently. *Adv. Mater.* **26**, 6829–6851 (2014).
12. Finch, C. M., García-Suárez, V. M. & Lambert, C. J. Giant thermopower and figure of merit in single-molecule devices. *Phys. Rev. B* **79**, 033405 (2009).
13. Bergfield, J. P., Solis, M. A. & Stafford, C. A. Giant thermoelectric effect from transmission supernodes. *ACS Nano* **4**, 5314–5320 (2010).
14. Snyder, G. J. & Toberer, E. S. Complex thermoelectric materials. *Nature Mater.* **7**, 105–113 (2008).
15. Harman, T. C., Taylor, P. J., Walsh, M. P. & LaForge, B. E. Quantum dot superlattice thermoelectric materials and devices. *Science* **297**, 2229–2232 (2002).
16. García-Suárez, V. M., Lambert, C. J., Manrique, D. Z. & Wandlowski, T. Redox control of thermopower and figure of merit in phase-coherent molecular wires. *Nanotechnology* **25**, 205402 (2014).
17. Stevenson, S. *et al*. Small-bandgap endohedral metallofullerenes in high yield and purity. *Nature* **401**, 55–57 (1999).
18. Nörenberg, C. *et al*. Self-assembly and electronic effects of $Er_3N@C_{80}$ and $Sc_3N@C_{80}$ on Au(111) and Ag/Si(111) surfaces. *J. Phys. Conf. Ser.* **100**, 052080 (2008).
19. Vacek, J., Vacek Chocholoušová, J., Stará, I. G., Starý a, I. & Dubi, Y. Mechanical tuning of conductance and thermopower in helicene molecular junctions. *Nanoscale* **7**, 8793–8802 (2015).
20. Paulsson, M. & Datta, S. Thermoelectric effect in molecular electronics. *Phys. Rev. B* **67**, 241403(R) (2003).
21. Agraït, N., Rubio, G. & Vieira, S. Plastic deformation of nanometer-scale gold connective necks. *Phys. Rev. Lett.* **74**, 3995–3998 (1995).
22. Rubio-Bollinger, G., Bahn, S. R., Agraït, N., Jacobsen, K. W. & Vieira, S. Mechanical propperties and formation mechanisms of a wire of single gold atoms. *Phys. Rev. Lett.* **87**, 026101 (2001).
23. Ruoff, R. S. & Ruoff, A. L. The bulk modulus of C_{60} molecules and crystals: A molecular mechanics approach. *Appl. Phys. Lett.* **59**, 1553–1555 (1991).
24. Ferrer, J. *et al*. GOLLUM: A next-generation simulation tool for electron, thermal and spin transport. *New J. Phys.* **16**, 093029 (2014).
25. Soler, J. M. *et al*. The SIESTA method for *ab initio* order-N materials simulation. *J. Phys. Condens. Matter.* **14**, 2745–2779 (2002).
26. Lambert, C. J. Basic concepts of quantum interference and electron transport in single-molecule electronics. *Chem. Soc. Rev.* **44**, 875–888 (2015).

Acknowledgements

This work was supported by the Swiss National Science Foundation (No. 200021-147143) as well as by the European Commission (EC) FP7 ITN 'MOLESCO' project no. 606728, UK EPSRC (grant nos. EP/K001507/1, EP/J014753/1, EP/H035818/1), Spanish MINECO (grant nos. MAT2011-25046 and MAT2014-57915-R), Comunidad de Madrid NANOFRONTMAG-CM (S2013/MIT-2850), MAD2D-CM (S2013/MIT-3007) and the Iraqi Ministry of Higher Education, Tikrit University (SL-20). L.R.-G. acknowledges financial support from UAM, IMDEA-Nanoscience and Spanish MECD (grant no. FPU014/03368). A.K.I. acknowledges financial support from Tikrit University.

Author contributions

L.R.-G. performed the experiments and analysed the experimental data. A.K.I. and I.G. carried out the theoretical calculations. K.P. purified and provided the endohedral molecules. C.E. contributed to the experiments and to the experimental set-up and G.R.-B. contributed to the experimental set-up. N.A. and C.J.L. conceived and supervised the experiment and wrote the manuscript with contributions from all the authors.

Additional information

Supplementary information is available in the online version of the paper. Reprints and permissions information is available online at www.nature.com/reprints. Correspondence and requests for materials should be addressed to N.A. or C.J.L.

Competing financial interests

The authors declare no competing financial interests.

Methods

STM measurements. The gold surfaces were flame-annealed before endohedral fullerenes were deposited, using the drop casting technique from solution in 1,2,4-trichlorobenzene (TCB) at very low concentration (10^{-7}–10^{-8} M). We used mechanically cut gold tips as STM probes. In order to measure the thermopower of molecular junctions, we modified our in-house-built STM set-up by adding a surface mount 1 kΩ resistor that acts as a heater for the tip holder[9], while the substrate was kept at room temperature. Two thermocouples connected to the tip holder and to the substrate surface were used to monitor the resulting temperature difference. Measurements were performed at a temperature difference of 40 K and at ambient conditions. We found that the temperature stabilizes in about 15–30 min. The error in the determination of the thermopower is about 0.6 μV K^{-1}. Further details are provided in the Supplementary Information.

Computational details. Electronic structure calculations were performed using the DFT code SIESTA (ref. 25). The optimum geometry of the C_{80} cage and encapsulated Sc_3N molecule was obtained by searching through atomic configurations until the lowest energy was found. In each case the molecule was relaxed until all the forces on the atoms were less than 0.05 V $Å^{-1}$. SIESTA employs pseudo-atomic orbitals and the relaxation was carried out using a double-zeta plus polarization orbital basis set. Norm-conserving pseudopotentials were used and an energy cutoff of 200 Ry defined the real-space grid. The exchange correlation functional used was the local density approximation (LDA). To calculate electron transport, the molecule was attached to gold leads and, owing to the large contact area of the C_{80} cage, a 5×6 atom layer of (111) gold was taken to be the surface of the lead. The optimum binding location was found by calculating the binding energy as a function of the separation distance z, taking into account basis set error corrections. Supplementary Fig. 6 shows that this distance is approximately 2.3 Å. The extended molecule included six layers of (111) gold and the Hamiltonian describing this structure was produced using SIESTA. The transmission coefficient $\mathcal{T}(E)$ and thermopower S were calculated using the Gollum code[24]. Further details are provided in the Supplementary Information.